19th International Conference on
Adaptive Structures and Technologies
October 6-9, 2008
Ascona, Switzerland

Modelling Continuously Morphing Aircraft for Flight Control

N. Ameri[1]*, M. I. Friswell[2], M. H. Lowenberg[3] and E. Livne[4]
[1] PhD student, Dept. of Aerospace Engineering, University of Bristol, Bristol, BS8 1TR, United Kingdom
[2] Professor, Dept. of Aerospace Engineering, University of Bristol, Bristol, BS8 1TR, United Kingdom
[3] Senior Lecturer, Dept. of Aerospace Engineering, University of Bristol, Bristol, BS8 1TR, United Kingdom
[4] Professor, University of Washington, Department of Aeronautics and Astronautics , Seattle, Washington 98195-2400, United States.

ABSTRACT

The goal of the present work is to develop a small-scale flying wing with active winglets from a discrete surfaces concept, actuated via single torque actuators, to a seamless continuous concept actuated via a distribution of actuators. A conceptual approach will allow the tailoring of the main parameters influencing the flexibility of the structures, via an efficient optimisation routine based on a certain actuation power requirement. The efficiency is guaranteed by the implementation of equivalent continuum models for the structure rather than a discrete finite element approach, while the aerodynamic loads are provided by the implementation of a vortex lattice code. The actuation can be provided either by piezo or thermo strain actuators. The paper describes the tools based on a static aeroelastic code which predicts the interaction of the actuated morphing wing and the flow field, and shows results from preliminary analysis.

Keywords: morphing aircraft, aeroservoelasticity, strain actuation, control.

1. INTRODUCTION

Morphing is the ability of a flying structure to achieve certain manoeuvres or performance specifications by means of in-flight shape changing. At the University of Bristol, Bourdin [1] developed a flying wing with independently tilted wing tips, where the active winglets allow basic manoeuvres to be performed. The configuration consists of a tapered-planar wing with no twist, 30 degree LE sweep angle and 1.8 m span. The model has two hinges parallel to the wing plane of symmetry while two separate actuators allow the winglets to rotate relative to the baseline thus modifying the dihedral angles.

The goal of the present work is to modify the flying wing with active winglets from the actual discrete surfaces concept, actuated via single torque actuators, to a seamless continuous concept actuated via a distribution of actuators (see Fig. 1). In order to achieve this goal, a more conceptual approach is needed. A conceptual approach will allow the tailoring of the main parameters influencing the flexibility of the structures, via an efficient optimisation routine based on a certain actuation power requirement. So far, the purpose of this work is to use equivalent plate continuum models to simulate morphing structures in the early design stages. This idea is reasonable as long as only global quantities of the response are of concern.

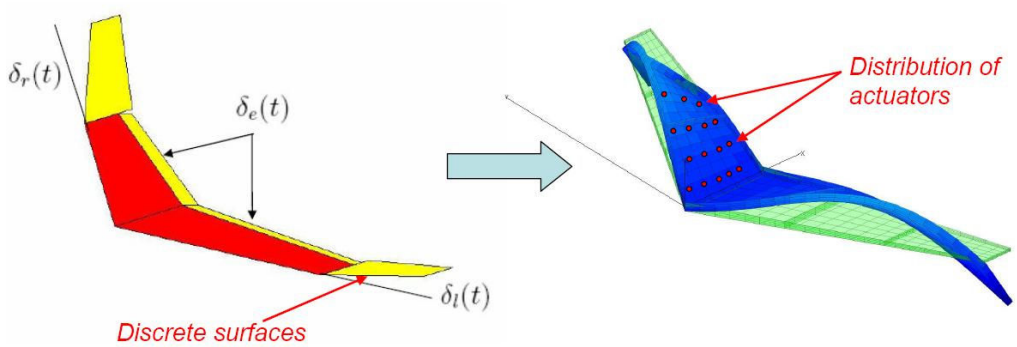

Figure 1. Discrete and continous morphing concept.

Equivalent plate capabilities for wing/control surface configurations have been investigated over the years for integrated aeroservoelastic flight vehicle design optimization at the conceptual design stage [2-8]. Even though they don't have the generality and power of finite element structural models, equivalent plate models have a number of attractive features such as low order models, as well as simplicity of parametrization for shape and sizing optimization. In aeroelastic/aeroservoelastic applications, because the displacement functions are continuous over the planform, the structural/aerodynamic interfacing is straightforward.

Some key challenges with equivalent plate models is the difficulty of capturing local effects. When simple polynomial Ritz base functions are used, the resulting numerical analysis is significantly simplified leading to explicit expressions of stiffness and mass matrix terms as functions of the system design variables. There is an ill-conditioning problem, however, when the order of polynomials used is higher than a certain threshold. Equivalent plate structural wing models have been known, therefore, to perform well in cases of smooth wing skin/web layups and distributed loading and actuation.

Another goal of the work is to investigate the potential of distributing strain actuators over wing/control surface configurations to achieve high effectiveness as in [9], where the articulated motion of control surfaces and strain actuated deformation were combined.

To allow inclusion in the design process of design variables that cover configuration planform shape as well as structural sizing design, composite material layout, and actuator distribution and command, an equivalent plate modeling approach has been under development. An assessment of the performance of this model, with initial results that focus on the static aeroelastic problem reported in Ref. [10]. For aeroelastic purposes a subsonic quasi-static 3D vortex lattice method has been implemented. Only a spanwise discretisation is taken into account so that the wing is divided into strips and for each strip induced drag, side force and lift can be evaluated. The new capability allows modeling of configurations made of articulated deformable segments undergoing small motions.

The paper is organized as follows. Section 2 provides a description of theoretical aspects of the equivalent plate modeling as well as the implementation of strain actuators. In sections 3 and 4, theoretical overviews of the vortex lattice method and of the aeroelasto-static system are provided, respectively. A detailed description of the theories implemented can be found in [10]. Finally in section 5 results from a preliminary parametric study are discussed.

2. STRUCTURAL MODELLING

An equivalent plate approach has been adopted for the structural part of the tool. The theory implemented, known as First Order Shear Deformation Theory (FSDT), relies on the Reissner-Mindlin [11, 12] model which relaxes the constraint that a normal to the mid-surface stays normal to the mid-surface after deformation, and a uniform transverse shear strain is allowed.

The theory can represent a generic thick trapezoidal wing made of spars, ribs and caps (see

Fig.2). Indeed, composite skins and fiber orientations can be included as design parameters. All of the main geometrical parameters such as skin, spar and rib thickness distribution, wing box depth distribution over the wing area and caps areas, are defined as simple polynomials over the trapezoidal area. For instance the skin thickness distribution t^i of the *i*-th layer can be defined as

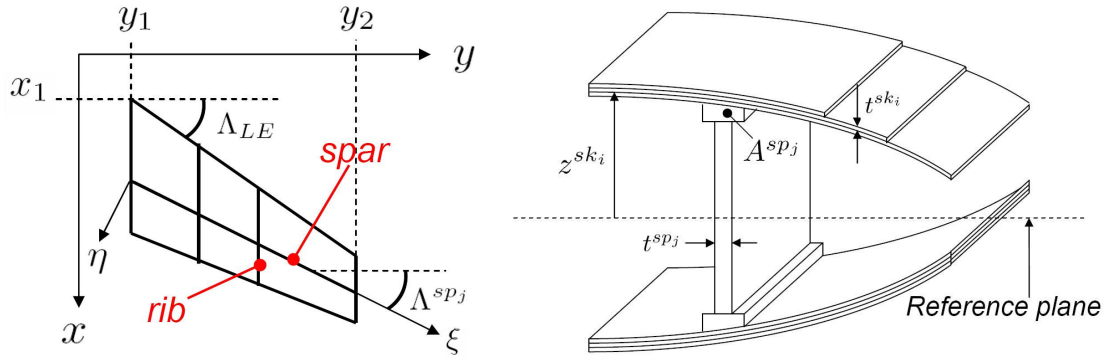

Figure 2. Generic trapezoidal wing (left) and wing box scheme (right) for equivalent plate modelling.

$$t^i(x,y) = \sum_{j=1}^{N} T_j \, x^{m_j} y^{n_j} \tag{1}$$

where the T_j coefficients can be used as design parameters.

In terms of constitutive properties, each skin layer has its own fibre direction defined over the *x* and *y* plane and under the hypothesis of small surface curvatures, the constitutive equations reflect a plane strain behavior ($\varepsilon_{zz} = 0$); the constitutive behaviour of spar and ribs, defined in local coordinates ξ and η, are such that only axial stress and transverse shear are sustained.

As previously stated the FSDT kinematic condition are based on the Reissner-Mindlin assumption, where the *u*, *v* and *w* displacements are approximated as

$$\begin{aligned} u(x,y,z,t) &= u_0(x,y,t) + z\varphi_x(x,y,t) \\ v(x,y,z,t) &= v_0(x,y,t) + z\varphi_y(x,y,t) \\ w(x,y,z,t) &= w_0(x,y,t) \end{aligned} \tag{2}$$

where u_0 v_0 and w_0 are displacements at the reference plane (*z*=0) while φ_x and φ_y are unknown functions representing the rotation of the sections about the *x* and *y* axes respectively. Indeed, the effect of shear deformation is included in those terms. The equivalent plate theory is based on the assumption that all of the deformation field is approximated by a series of Ritz polynomials. Thus all of the displacements at the reference plane, as well as the rotation functions can be defined as a combination of polynomial shape functions whose coefficients can be regarded as generalised displacements for the system. Eq. (2) can be written as

$$\mathbf{u}(x,y,z,t) = \mathbf{S}(x,y,z)\,\mathbf{q}(t) \tag{3}$$

where $\mathbf{u}$ is the vector collecting the displacements, $\mathbf{S}$ is the matrix collecting the shape functions and $\mathbf{q}$ is the vector of generalised coordinates.

Finally, in order to evaluate mass and stiffness matrices, an energy approach is adopted. Firstly, kinetic and potential energies of infinitesimal elements belonging to each structural element comprising the wing box are evaluated, and then an intergration over the skin, spar, rib and cap volumes is perfomed in order to evaluate the total system energies. The main advantage of the

equivalent plate modeling is that the intergration is performed analytically as only polynomials are involved, and in closed form, without the need of numerical integration. A symbolic tool, such as Maple, is used to evaluate the integrals. Once the energy variational is evaluated, the Lagrange equation will lead to the equilibrium equation

$$\mathbf{M}\ddot{\mathbf{q}} + \mathbf{K}\mathbf{q} = \mathbf{e} \tag{4}$$

where the mass ($\mathbf{M}$) and stiffness ($\mathbf{K}$) matrices are evaluated in closed form, and $\mathbf{e}$ is the vector of the generalised external forces. The expressions are then exported to Matlab in order to have functions such as

$$\begin{aligned} \mathbf{M} &= \mathbf{M}(\rho, c, \Lambda_{LE}, b, h, N^{Spar}, N^{Rib}, ...) \\ \mathbf{K} &= \mathbf{K}(E, \nu, b, \Lambda_{LE}, N^{Spar}, N^{Rib}, ...) \end{aligned} \tag{5}$$

that provide the system matrices as a function of all of the design parameters.

2-1. Multiple plate capabilities

If the system comprises of more than one plate, each of them with arbitrary orientation in space, a global coordinate system has to be set up. A local coordinate system, fixed with respect to the undeformed reference state, can be defined for each plate. Thus if the same set of polynomials is used for each plate, the global number of degrees of freedom will $N_P \times N_q$ where N_P is number of plates and N_q is the number of degrees of freedom of each plate. Finally each plate will add to the system a contribution to the kinetic and potential energies that is evaluated with respect to the local coordinate system and thus the formulation obtained in previous sections will be used for this purpose.

In the current formulation the displacement compatibility between contiguous plates is imposed by means of stiff springs. Demasi [13] used only longitudinal springs placed throughout the thickness to impose the cantilever condition and the compatibility, however both rotational and longitudinal springs will be used in this work. Each set of springs introduces a contributions to the stiffness matrix of each plate and a cross contribution between plates so that the global stiffness matrix of dimension $(N_P \times N_q) \times (N_P \times N_q)$ may be assembled. The mass matrix can be assembled in a similar way but no cross contribution will appear.

2-2. Piezo and thermo actuator modelling for the equivalent plates

A patch of piezo or thermo actuator undergoes a strain variation when an electrical field or a thermal variation respectively, is imposed through the thickness. Assuming that the patches are thin enough to be modelled as plates and assuming a plane-strain behavior, the previous relations can be expressed analytically by the following

$$\widetilde{\boldsymbol{\varepsilon}}_{\Delta T} = \begin{bmatrix} \varepsilon_{11} \\ \varepsilon_{22} \\ \gamma_{12} \end{bmatrix} = \begin{bmatrix} \alpha_1 \\ \alpha_2 \\ 0 \end{bmatrix} \Delta T, \quad \widetilde{\boldsymbol{\varepsilon}}_{V} = \begin{bmatrix} \varepsilon_{11} \\ \varepsilon_{22} \\ \gamma_{12} \end{bmatrix} = \begin{bmatrix} d_{13} \\ d_{23} \\ 0 \end{bmatrix} \frac{V}{t} \tag{6}$$

where $\tilde{\boldsymbol{\varepsilon}}_{\Delta T}$ and $\tilde{\boldsymbol{\varepsilon}}_{V}$ are the strains defined in the principal material coordinates of each patch, α_1 and α_2 [C^{-1}] are the thermal expansion coefficients in the 1 and 2 directions respectively, d_{13} and d_{23} [m/V] are the piezoelectric constants; ΔT is the temperature variation input with respect to a reference temperature, while the ratio V/t, between the input voltage V and the distance between the electrodes t, represents the through-thickness electric field.

The strain due to the stress field $\boldsymbol{\varepsilon}_S$ is obtained by subtracting from the total strain field $\boldsymbol{\varepsilon}$ the contribution due to the thermal and the piezoelectric strains in global coordinates. Thus

$$\boldsymbol{\varepsilon}_S = \boldsymbol{\varepsilon} - \boldsymbol{\varepsilon}_{\Delta T} - \boldsymbol{\varepsilon}_V \tag{7}$$

The equations describing the interaction between the smart patches and the structure will be obtained via a virtual work approach. The virtual work is evaluated as follows

$$\begin{aligned} \delta W_{\varepsilon} &= \delta \boldsymbol{\varepsilon}^T \boldsymbol{\sigma}\, t\, dx\, dy \\ \delta W_i &= \delta \mathbf{u}^T \mathbf{f}_i = -\rho \delta \mathbf{u}^T \ddot{\mathbf{u}}\; t\, dx\, dy \\ \delta W_{ext} &= \delta \mathbf{u}^T \mathbf{f}_{ext}\, dx\, dy \end{aligned} \tag{8}$$

where δW_{ε} is the virtual work done by the stresses $\boldsymbol{\sigma}$, δW_i the virtual work done by the inertial forces $\mathbf{f}_i$, calculated using d'Alembert's principle, and δW_{ext} is the work done by the external forces $\mathbf{f}_{ext}$ per unit area. The equilibrium condition, which states that the external and inertial virtual work must balance the internal work done by the stresses, leads to the equilibrium equation for the strain actuator

$$\mathbf{M}^A \ddot{\mathbf{q}} + \mathbf{K}^A \mathbf{q} = \mathbf{e}_{ext} + \mathbf{e}_V V + \mathbf{e}_{\Delta T} \Delta T \tag{9}$$

where $\mathbf{M}^A$ and $\mathbf{K}^A$ are the mass and stiffness contribution of the strain actuator to be added to the total mass and stiffness matrix of the structure, while $\mathbf{e}_V$ and $\mathbf{e}_{\Delta T}$ are the generalized vectors providing to the structure the effect of an applied voltage and a temperature variation, respectively. If several actuators are placed over the wing surface, the contribution of each actuator has to be included.

3. AERODYNAMIC MODELLING

The VLM assumes incompressible potential and quasi-steady aerodynamics in which the wing surface is subdivided into panels. Each panel carries a horseshoe vortex inducing velocities throughout the field and particularly to the other panels. The velocities induced by each vortex are evaluated at certain control points using the Biot-Savart law; the satisfaction of the no-flow-through condition for the wing at these points yields a set of linear algebraic equations which provides the strength of the vortices, given the free stream velocity U_∞, the angle of attack α and the wing shape.

For the sake of the present work only a spanwise discretisation is considered, and thus the wing is sub-divided into strips each carrying a horseshoe. The bound vortex filament coincides with the quarter-chord line and the left-hand and right-hand vortex filaments lay on the panel surfaces. The trailing vortices leaving the wing are assumed to be parallel to the *x* axis of the wing as a linearized approach is adopted. Finally, the control point of the panel is located at the three-quarter-chord.

The velocity induced on a generic point a'' in the space by a finite vortex filament of strength

Γ and limit *a a'*, is given by applying the Biot-Savart law.

$$\mathbf{w} = \frac{\Gamma}{4\pi} \frac{\mathbf{r}_1 \times \mathbf{r}_2}{|\mathbf{r}_1 \times \mathbf{r}_2|} \left[\mathbf{r}_0 \cdot \left(\frac{\mathbf{r}_1}{r_1} - \frac{\mathbf{r}_2}{r_2} \right) \right] \tag{10}$$

Where r_1 and r_2 are the magnitudes of the vectors $\mathbf{r}_1$ and $\mathbf{r}_2$ respectively. This expression can be used to calculate the velocity at the control point of the *m*-th panel induced by the horseshoe belonging to the *n*-th panel. This leads to the calculation of the influence matrices which provide, given the vector collecting the vortex strengths of each panel $\mathbf{\Gamma}$, the vectors of the *x*, *y* and *z* component of the induced velocities. The vortex strengths are found by solving the linear system of equations

$$\mathbf{A}\,\mathbf{\Gamma} = U_\infty \mathbf{b} \tag{11}$$

obtained by applying the no-flow-through condition on each panel. Note that the $\mathbf{A}$ matrix is a non-linear function of the geometric parameters while the $\mathbf{b}$ vector also depends on the angle of attack. Once the vortex strengths are obtained, the loads on each panel are calculated by applying the generalised Kutta-Joukowsky law [14] at the mid-point of the quarter-chord bound vortex, in the form

$$\mathbf{f}_m = \rho \Gamma_m \left(\mathbf{u}_\infty + \mathbf{w}_{1/4} \right) \times \mathbf{l} \tag{12}$$

where $\mathbf{l}$ is the vector along the quarter-chord line of the panel, $\mathbf{u}_\infty$ is the free stream velocity expressed in global coodinates and $\mathbf{w}_{1/4}$ is the induced velocity at the mid-point of the quarter-chord bound vortex. Expression (12) provides loads in the global coordinate system and takes into account the induced drag effect.

4. STATIC AEROELASTIC SYSTEM

In this section the structural and aerodynamic tools previously developed are linked together, in order to generate the static aeroelastic system. The aerodynamic loads acting on the wing depend on how the flow field is affected by the wing geometry. Because the wing is not rigid, the loads acting on the wing surface induce a deformation of the wing. This change in shape affects the original flow ield, leading to a feedback-loop between aerodynamics and the structure.

The matrix of influence coefficients $\mathbf{A}$ in Eq. (11) depends on the geometric configuration and thus on the wing shape. A certain number of displacements and the direction cosines locate and orientate each panel in space. Those quantities depend on the generalised coordinates. Using the Kutta-Joukowsky law given by Eq. (12), the aerodynamic force vector $\mathbf{f}_m$ on the *m*-th panel can be evaluated as a non-linear function of the generalised coordinates. The overall aerodynamic load distribution on the panels can be regarded as a distribution of concentrated loads.

The equations governing the static equilibrium of the servo-aero-elastic systemsystem is obtained considering Eqs. (4) and (9), as

$$\left(\mathbf{K}^A + \mathbf{K} \right) \mathbf{q} = \mathbf{e}_{aer}(\mathbf{q}) + \mathbf{e}_{ext} + \mathbf{e}_V V + \mathbf{e}_{\Delta T} \Delta T \tag{13}$$

where $\mathbf{e}_{aer}$ is the vector of the generalised aerodynamic forces.

5. PRELIMINARY RESULTS

The effect of some design parameters on the aerodynamic coefficients is discussed in this section. The wing under investigation is a 30° leading edge swept-back wing, with 0.3 m of aerodynamic chord at the root, a taper ratio of 0.33, and 1.9 m of span, *b*. The wing box has a structural chord that is 50% of the local aerodynamic chord, while the depth is 7%. A hinge placed at 75% of the span, splits the the wing into an inner (the baseline) and an outer (the winglet) portion. The hinge angle δ_w, and thus the winglet position, can be varied by means of a torque actuator. A total number of 5 ribs, equaly spaced, are placed within the baseline, while 3 ribs are allocated for the winglet. The wing box is entirely realised in Kevlar Epoxy composite (see Tab. **Error! Reference source not found.**). All the ticknesses are set to $t = 1$ mm, while the cap areas are set to 25×10^{-6} m^2 The wing is set to fly at a speed of $U_\infty = 30$ m/s, and at an angle of attack of $\alpha = 3°$ at sea level. The aerodynamic loads are based on 10 panels for inner wing and 6 for the outer. An overall structural and aerodynamic symmetry condition about the x-z plane is assumed.

A type of piezoceramic composite actuator commonly known as a Macro Fiber Composite (MFC) is used for the present simulations. The MFC, developed at NASA Langley Research Center [15], is a layered, planar actuation device that employs rectangular cross-section, unidirectional piezoceramic fibers (PZT 5A) embedded in a thermosetting polymer matrix. This active, fiber reinforced layer is then sandwiched between copper-clad Kapton film layers that have an etched interdigitated electrode pattern. Because of the in-plane poling the MFC uses the d_{33} piezoelectric

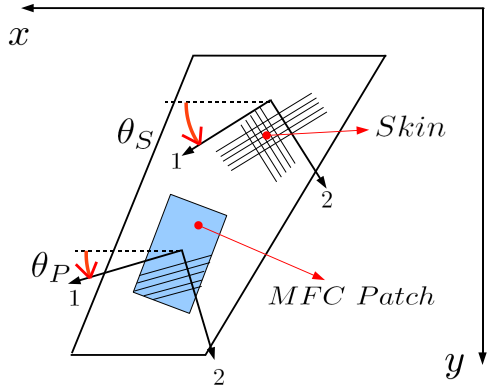

Figure 3. Skin and MFC fiber layout on the winglet.

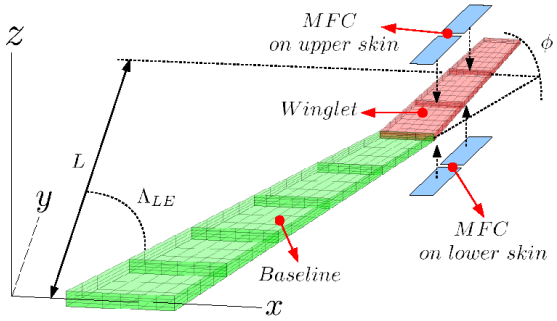

Figure 4. Wing box scheme.

		MFC	Kevlare-Epoxy
E_1	[GPa]	30.3	75.8
E_2	[GPa]	15.9	5.5
ν_{12}	[-]	0.31	0.27
G_{12}	[GPa]	5.52	7.2
ρ	[Kg/m^3]	4700	1380
d_{13}	[m/V]	$4.6\ 10^{-10}$	
d_{23}	[m/V]	$-2.1\ 10^{-10}$	
T	[m]	$0.3\ 10^{-3}$	
$\Delta\chi$	[m]	$0.5\ 10^{-3}$	

Table 1. Main material properties of the Macro Fiber Composite (MFC) actuator and Kevlar Epoxy skin composite.

effect, which is much stronger than the d_{31} effect used by traditional PZT actuators with through-thickness poling.The MFC patches work in a voltage range of -500 to 1500 V and the main parameters are given in Tab. **Error! Reference source not found.**, (see Ref. [16]), where T is the actuator thickness and $\Delta\chi$ is the distance betwee the electrodes.

5-1. Effect of composites layout

A total number of four MFC patches of dimension 0.056×0.085 m, are placed on the winglet. Specifically, two of them are placed on the upper surface, along the elastic axis direction, and loaded with the maximum positive voltage of 1500 V; the other two are placed on the lower skin and loaded with the maximum negative voltage -500 V. The goal is to investigate the effect of the skin and piezo-patch orientations, identified by the angles ϑ_S and ϑ_P respectively, on the aerodynamic coefficients. The local material coordinate system of the skin and the piezo-patches are given in Fig. 3, while a scheme for the whole configuration is given in Fig. 4. The winglet is fixed at δ_w=15°. The aerodynamic coefficients are evaluated with respect to the same reference length, namely the wing span of the unfolded configuration.

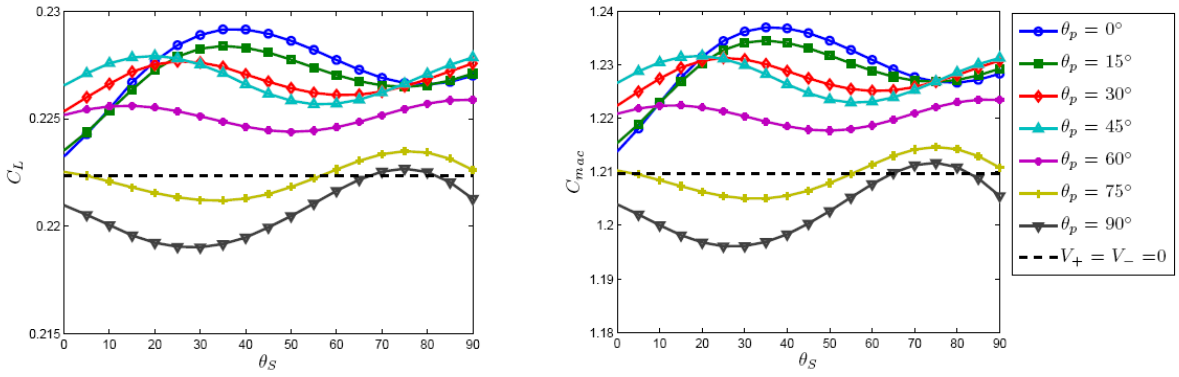

Figure 5. Lift and moment coefficients as a function of the MFC and skin web layouts.

Results from the simulations are given in Fig. 5, where the aerodynamic coefficient C_L and the pitching moment coefficient C_{mac} about the aerodynamic centre, are given as a function of ϑ_P and ϑ_S Moreover, the values of the coefficients evaluated when no voltage input is given to the patches, are set to be the reference values in each diagrams. These reference coefficients, which are due only to the fluid-structure interaction, are minimally affected by the composite web angles, and thus are evaluated as the mean value over the angles domain. The results can be summarised as follows:

1. for ϑ_S=37° and ϑ_P=0° the maximum positive variation occurs; this combination of angles causes the winglet to twist with a positive angle, and thus to increase the local angle of attack.
2. for ϑ_S=30° and ϑ_P=90° the maximum negative variation; the winglet undergoes to negative torsion that decreases the local angle of attack.

Values for those two cases are reported in Tab 2.

ϑ_S [°]	ϑ_P [°]	ΔC_L [%]	ΔC_{Di} [%]	ΔC_{mac} [%]
37	0	3.12	7.90	2.31
30	90	-1.55	-2.74	-1.32

Table 2. Aerodynamic coefficient variations for two sets of piezo and skin layout.

5-2. Effect of thickness and depth parameters

In this section the effect of the skin and spar thickness (t) and the wing box depth (h) parameters on the aerodynamic coefficients are discussed. The configuration is the same as adopted in the previous section, where the skin and MFC fiber layout is set to ϑ_S=37° and ϑ_P=0° which provides the maximum variation of the aerodynamic coefficients. It has to be pointed out that, because of the reliminary nature of the investigation, no buckling analysis has been undertaken for the current simulation.

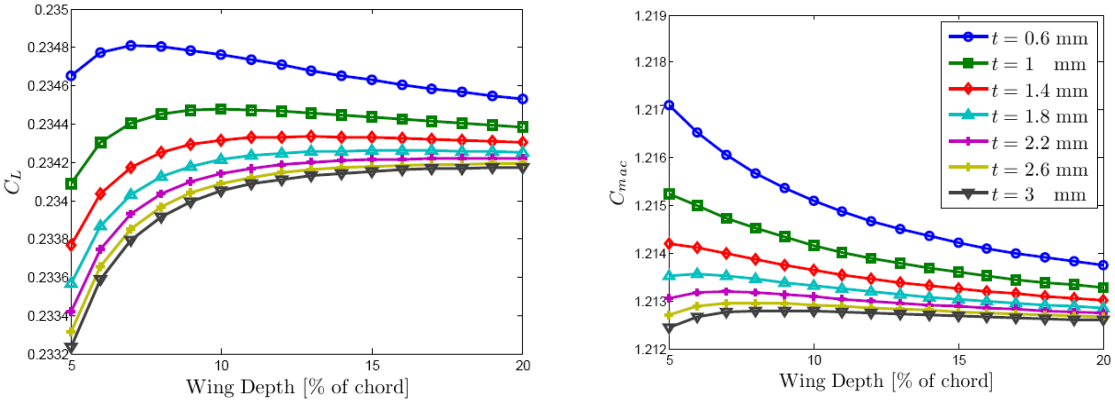

Figure 6. Lift (left) and moment (right) coefficients as a function of the thickness and wing-box-depth parameters.

For the current analysis, the range of wing depths chosen goes from 5 to 20% of the aerodynamic chord, while, for each of these values, the thickness varies from 0.6 to 3 mm. Results are given in Fig. 6, for the lift and the moment coefficients about the aerodynamic centre. The results can be summarised as follows:

1. for very thin skins (t < 1 mm), the lift coefficient exhibits a local maximum with respect to the wing box depth. Thus after an initial increase, the lift coefficient starts to decrease. For thick skins (t > 1 mm) the lift coefficient increases with the wing box depth.
2. for thin skins (t < 2.2 mm), the moment coefficient decreases with wing box depth, while for thick skins (t > 2.2 mm) the moment coefficients has a local maximum.

These behaviors may be explained by the variation of the torsional stiffness, and in particular the polar inertia of the rectangular section, with wing box depth and skin thickness.

6. CONCLUSIONS

The paper presents a computational approach for an integrated aeroservoelastic modeling of strain actuated wings, addressed to preliminary conceptual design of morphing aircraft. The approach relies on continuum modeling based on an equivalent plate model approach for the structural modeling, and a subsonic quasi-static 3D vortex lattice method for the aerodynamic load. Finally an

example of the capability of the code has been given.

Future developments include:

1. a genetic algorithm (GA), can be implemented to find the best combination of composite material orientation, wing geometry and actuator positions which minimises the energy required to achieve a certain wing shape, and thus a certain manoeuvre. It is also possible to consider other cost functions such as the lift to drag ratio.
2. In order to deal with aeroelastic response problems an unsteady aerodynamic code needs to be implemented: this could be ether a simple 2D Theodorsen strip method, as a first step, or a more sophisticated 3D unsteady panel methods. Finally the actuation scenario can be extended in order to include point-to-point truss-actuators.

ACKNOWLEDGEMENTS

This work has been supported by a Marie-Curie excellence research grant funded by the European Commission, and a Worldwide University Network (WUN) funding.

REFERENCES

1. P. Bourdin, A. Gatto, M.I. Friswell. "The Application of Variable Cant Angle Winglets for Morphing Aircraft control", 24th Applied Aerodynamics Conference, San Francisco, California AIAA paper 2006-3660.
2. R. W. Lynch, W. A. Rogers, "Aeroelastic Tailoring of Composite Materials to Improve Performance", AIAA-1976-1505, ASME, and SAE, Structures, Structural Dynamics, and Materials Conference, 17th, King of Prussia, Pa.
3. G. L. Giles, "Further generalization of an equivalent plate representation for aircraft structural analysis", Journal of Aircraft 1989, vol.26 no.1, pp. 67-74.
4. R. K. Kapania, and S. Singhvi, "Free Vibration Analyses of Generally Laminated Tapered Skew Plates", Composites Engineering, Vol. 2, No. 3, 1992, pp. 197212.
5. E. Livne, "Equivalent Plate Structural Modeling for Wing Shape Optimization Including Transverse Shear", AIAA Journal, Vol. 32, No. 6, 1994, pp. 1278-1288.
6. E. Livne, L. A. Schmit, Jr., and P. P. Friedmann, "Integrated structure /control /aerodynamic synthesis of actively controlled composite wings", Journal of Aircraft 1993, vol.30, no.3, pp. 387-394.
7. R. K. Kapania and Y. Liu, "Static and Vibration Analyses of General Wing Structures Using Equivalent-Plate Models", AIAA Journal, Vol. 38, No. 7, July 2000, Virginia Polytechnic Institute and State University, Blacksburg, Virginia 24061.
8. T. Krishnamurthy, and F. Tsai, "Static and Dynamic Structural Response of an Aircraft Wing with Damage Using Equivalent Plate Analysis", AIAA-2008-1967 49th AIAA/ASME/ASCE/AHS/ASC Structures, Structural Dynamics, and Materials Conference 16th AIAA/ASME/AHS Adaptive Structures Conference 10t, Schaumburg, IL, Apr. 7-10, 2008
9. T. Jackson, and E. Livne, "Integrated Aeroservoelastic Design Optimization of Actively-Controlled Strain-Actuated Flight Vehicles", AIAA-2005-2170, 46th AIAA/ASME/ASCE/AHS/ASC Structures, Structural Dynamics and Materials Conference, Austin, Texas, Apr. 18-21, 2005.
10. N. Ameri, M. Lowenberg and M. Friswell, E. Livne, "Modelling Continuously Morphing Aircraft for Flight Control", AIAA-2008-6966, AIAA Guidance, Navigation and Control Conference and Exhibit, Honolulu, Hawaii, Aug. 18-21, 2008.

11. E. Reissner, “The Effect of Transverse Shear Deformation on the Bending of Elastic Plates”, Journal of Applied Mechanics, Vol. 12, 1945, pp. A-69~77.
12. R. D. Mindlin, “Influence of Rotatory Inertia and Shear on Flexural Motions of Isotropic, Elastic Plates”, Journal of Applied Mechanics, Vol. 18, 1951, pp. 31-38.
13. L. Demasi and E. Livne, “Structural Ritz-Based Simple-Polynomials Nonlinear Equivalent Plate Approach - An Assessment”, 46thAIAA/ASME/ASCE/AHS/ASC Conference, April 18-21, 2005, Austin, Texas, AIAA 2005-2093.
14. P. G. Saffman, “Vortex Dynamics”, Cambridge Univeristy press
15. W. K. Wilkie, G. R. Bryant, J. W. High,, “Low-Cost Piezocomposite Actuator for Structural Control Applications”, SPIE 7th Annual International Symposium on Smart Structures and Materials, Newport Beach, CA, 2000.
16. www.smart-material.com